JOURNAL OF SPACECRAFT AND ROCKETS
Vol. 41, No. 5, September–October 2004

Power Reduction of Solar Arrays by Arcing Under Simulated Geosynchronous Orbit Environment

Kazuhiro Toyoda,* Toshiaki Matsumoto,† and Mengu Cho‡
Kyushu Institute of Technology, Kitakyushu 804-8550, Japan
Yukishige Nozaki§
NEC Toshiba Space Systems, Ltd., Yokohama 224-8550, Japan
and
Masato Takahashi¶
National Space Development Agency, Ibaraki 305-8505, Japan

Engineering Test Satellite VIII, which is a geosynchronous orbit satellite operated with 110-V bus voltage, will be launched in 2004. Laboratory tests on charging and arcing of engineering-test-satellite solar arrays are carried out in a simulated geosynchronous orbit environment irradiating a solar-array test coupon with an electron beam in a vacuum chamber. Long-duration experiments are carried out using the insulation-reinforced coupons with thick silicon adhesive layer to verify the insulation capability. The test coupons have the electric power drop caused by contamination of the coverglass surface and the destructive damage of cell. The power drop is not related to voltage between adjacent cell strings. It is confirmed that the power drop occurs regardless of the thickness of adhesive layer, although thick room-temperature-vulcanization silicon adhesive coating leads to more contamination. Based on the test results, the final array design for Engineering Test Satellite VIII is determined.

Introduction

INCREASE in the electric power required by a satellite leads to an increase in the bus voltage of a satellite. Recently, many satellites have been designed to operate at high voltage of over 100 V. The high voltage generated by solar arrays, however, can cause catastrophic damage such as that from short circuit because of sustained arcs.[1] Therefore, it is important to prevent the occurrence of a sustained arc for reliable power generation.

The National Space Development Agency of Japan plans to launch the Engineering Test Satellite VIII (ETS-VIII), a 3-ton class geosynchronous orbit (GEO) satellite with a design lifetime of 10 years. ETS-VIII will test new technologies such as high-voltage bus technology (100 V) and a large-scale deployable reflector made of gold mesh. This flight will establish and verify the technology for future large-scale spacecraft systems.[2]

Arcing on the high-voltage solar array of ETS-VIII has been studied by previous investigations.[3,4] The negative end of solar array is usually connected to the ground provided by the spacecraft body. In GEO, arcing as a result of the space plasma is very rare under normal condition because the plasma density is much smaller than that in low Earth orbit (LEO). However, a substorm can cause the arcing on solar arrays in GEO by producing the high-energy electrons of greater than 10 keV. When a satellite encounters the substorm, its potential can drop to a negative potential if the influx of electrons exceeds the photoelectron emission. The emission of secondary electrons from the coverglass can be larger than that from the satellite body. Under such a condition, the coverglass potential can be less negative than the nearby conductor potential. This potential gradient between the coverglass and interconnectors is sometimes called inverted potential gradient. This condition is equivalent to the coverglass charging caused by plasma in LEO. Once the inverted potential gradient is formed, an arc can occur even in the GEO environment. On the inverted potential gradient condition, the coverglasses have positive charge and produce a strong electric field on the triple junction, which is formed by the interconnector, the coverglass, and the space. It is thought that these phenomena cause arcs on the solar array. However, even if an arc occurs, it causes little harm as long as it ends as a single pulse with a small amount of total energy release. In this paper, we call such a single arc pulse a trigger arc.

In the previous studies on the ETS-VIII solar arrays,[3,4] we found two serious types of damage on the solar array and proposed new array designs to protect against such damage. One of the types of damage is the intrastring sustained arc. Figure 1 shows the layout of ETS-VIII solar-array strings. The potential is 0 V at the negative end and 110 V at the positive end. Therefore the maximum potential difference between adjacent cells is 55 V. When a trigger arc occurs between strings with a differential potential, the arc can be sustained by receiving the power generated by the solar-array strings. The arc current keeps flowing, and the underlying Kapton insulation layer is thermally broken leading to the permanent short circuit between the array string and the substrate. In the present paper, we call this type of sustained arc an interstring sustained arc. The TEMPO-2 satellite experienced the permanent loss of a significant fraction of its solar-array output power in 1997. Katz et al.[1] attributed the failure to the interstring sustained arc. In our ground experiments,[4] we confirmed that interstring sustained arc occurred with the differential potential of 55 V and the current of 2.64 A in a simulated LEO condition.[4] To mitigate the risk from this type of sustained arc, we grouted the gap between strings with room-temperature vulcanization (RTV) silicon adhesive. Consequently, the solar array withstood breakdown up to the interstring voltage of 120 V (Ref. 4).

Another type of destructive damage is caused by the sustained arc between the interconnector and the panel structure, possibly through an insulation defect in the Kapton sheet on which solar cells are mounted. MARCES-A and ECS-1 experienced partial loss of power, which was attributed to a short circuit between the array

Received 19 November 2002; revision received 8 September 2003; accepted for publication 9 September 2003.

*Postdoctoral Fellow, Satellite Venture Business Laboratory; currently Research Associate, Chiba University, Inage-ku, Chiba 263-8522, Japan; toyoda@faculty.chiba-u.jp. Member AIAA.

†Graduate Student, Department of Electrical Engineering; currently Power Electronics Engineering/Electrical Design Engineer, Mitsubishi Electric Logistics Support Co., Ltd., Kamimachiya, Kamakura, Kanagawa 247-0065, Japan.

‡Associate Professor, Department of Electrical Engineering, Tobata-ku; cho@ele.kyutech.ac.jp. Member AIAA.

§Assistant Manager, Electrical Systems Department, System Development Division, Tsuzuki; nozaki.yukisige@ntspace.jp.

¶Associate Senior Engineer, Tsukuba; Takahashi.Masato@nasda.go.jp.

and the panel structure through a damaged Kapton sheet.[5] There are several ways for Kapton to be damaged, such as accidental scars caused by workmanship during the cell repair process on the ground or debris impact in orbit. Once an arc occurs near the damaged Kapton, a current path can be formed between the interconnector and the substrate through the damaged portion of the Kapton leading to a short circuit between the interconnector and the substrate, resulting in the loss of the power system.[5] We call this type of sustained arc as string-substrate sustained arc in this paper. We performed a ground-based experiment to verify the string-substrate sustained arc.[3] We intentionally damaged the Kapton near interconnector and initiated arcs on the solar array using an electron beam.[3] Consequently, we verified that the string-substrate sustained arc occurred at 110 V and 2.64 A and showed that this type of sustained arc could result from the inverted gradient condition in GEO. Without defects on the Kapton sheet, this string-substrate sustained arc never occurred under the same conditions. To provide an additional safety margin, we proposed a new array design, which had thicker RTV between cells and the Kapton sheet and had RTV covering the Kapton sheet even under the interconnector to enhance the insulation between strings and substrates.

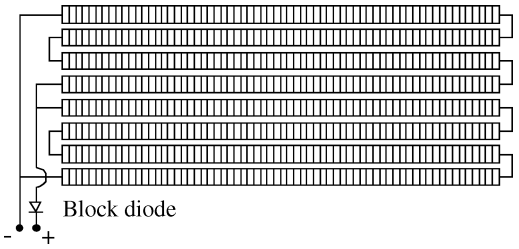

Fig. 1 Layout of the ETS-VIII solar-array strings.

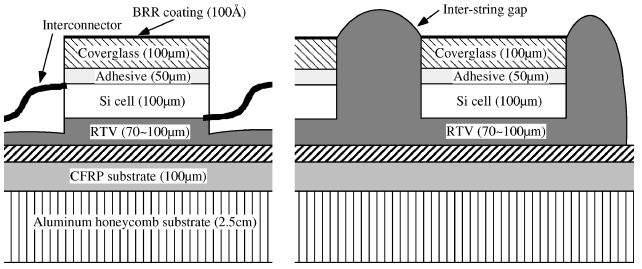

a) Cross section of thick coupon

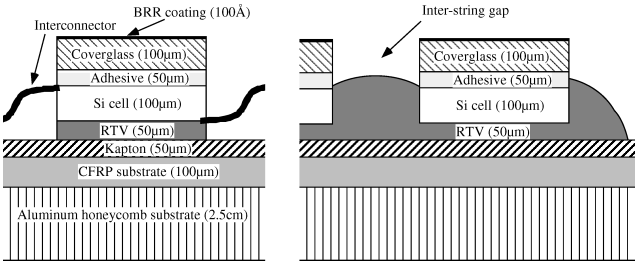

b) Cross section of thin coupon

Fig. 2 Sectional view of thick and thin coupons.

The primary purpose of this study was to verify that the newly designed insulation-reinforced array shows no peculiar behavior under the GEO environment. In the present work, we tested two types of array coupons. The secondary purpose was to investigate the effect of RTV coating by comparing two array designs with different degrees of RTV coating. We studied whether the thicker RTV coating always provided the better solution.

The two types of test coupons had different thicknesses of RTV silicone adhesive between the cell and the Kapton sheet. We refer to the coupon with thicker RTV as a thick coupon and the other coupon as a thin coupon. The thin coupon was the same type used in a previous investigation.[3] Figure 2 shows a sectional view of the thick and thin coupons. The RTV protruded under interconnectors from the bottom of cells. In a previous investigation, we confirmed that the string-substrate sustained arc occurred on the solar array with scratches on the Kapton sheet near interconnectors.[3] Thicker RTV was applied to prevent this sustained arc. The RTV grouting between strings was also made thicker. We used two thick coupons and a thin coupon in the experiments. For the thin coupon, there is no RTV below interconnector. For thick coupons, integrated bypass function (IBF), which will be used in the flight model, is adopted in the cells. The IBF allows a current to flow from the N to the P electrode through the cells and prevents the large inverse voltage from being applied between both end of the cells, even if the cells can not generate the electrical power.

To distinguish each coupon, we refer to the two thick coupons as thick-1 and thick-2, respectively, and refer to the thin coupon as thin-1. Three coupons were tested in a vacuum chamber simulating the GEO environment during a substorm by using an electron beam.

In the following sections of the paper, we describe the experimental results. After the experiments, both contamination of the coverglass surface and cell damage were observed, and the electrical power output of the array coupons decreased. We discuss the causes of these phenomena and describe the final array design for the flight model.

Experiment

Experimental Setup

A schematic picture of the experimental setup is shown in Fig. 3. The solar-array coupon is suspended with wires at four corners of the array. The vacuum chamber is 1 m in diameter and 1.2 m in length. The solar-array coupon is electrically insulated from the chamber. A power supply is used to set the potential of the solar array frame and the solar cells to −3 kV. The vacuum chamber is evacuated using a turbomolecular pump and reaches approximately

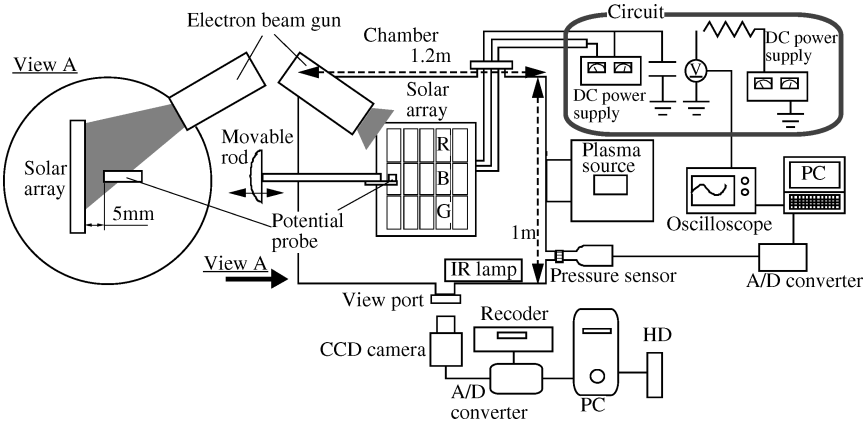

Fig. 3 Schematic picture of experimental setup.

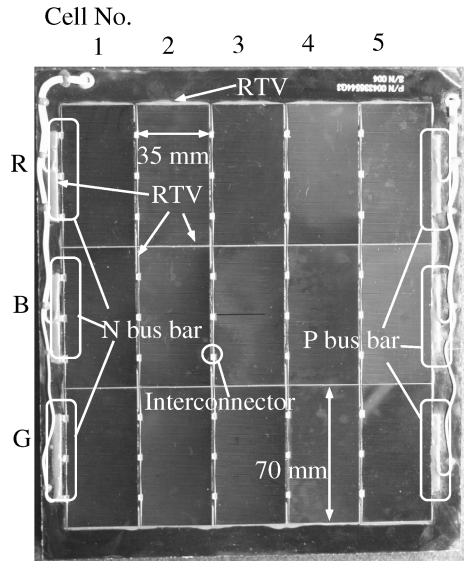

Fig. 4 Photograph of solar-array coupon used in experiments.

3×10^{-4} Pa before the experiment. During the experiment, a typical pressure is 7×10^{-4} Pa, and the neutral density is 2×10^{17} m^{-3}.

The electron beam is used to set the coverglass potential to more positive than the cells to provide the inverted gradient condition. The electron gun is fixed in the vacuum chamber and can produce an electron beam with an energy up to 30 kV. The electron beam has a half-width of approximately 9 cm at the array position. The maximum beam current density is about 6 mA/m^2 at 5 kV at the array position. Because of limitations imposed by the chamber geometry, the beam hits the array at an angle of 40 deg.

The potential on the surface of the array is measured using a noncontacting surface potential probe. This probe is capable of measuring a potential in the range of ± 20 kV. The probe is fixed on a movable rod and moved over the center string (B string in Fig. 4) along the center axis of the vacuum chamber while maintaining a distance of 5 mm from the solar-array surface.

Arc locations on the solar arrays are identified by digitally processing the video image. The video image taken by a digital video camera is sent to a PC and is recorded into a hard disk drive connected to the PC. After the experiments, arc locations are identified by analyzing the digital video image using a computer program on the PC. An 80-GB hard disk can record the digital video image for a duration of about 6 h.

Solar Array

The ETS-VIII satellite has 88 strings (two wings), each with 262 Si-IBF solar cells. Each string produces the output voltage of 110 V and is configured in four rows of 66 cells. Two strings are connected together in the harness with a block diode at the positive end. The gaps between adjacent cells are potted with nonconductive RTV silicon (Si) adhesive. Each string will produce approximately 1.32 A of current under optimal conditions. The ETS-VIII array layout has adjacent cells with a 55-V maximum potential difference and a maximum current capability of 2.64 A. The layout of two array strings is shown in Fig. 1. The coverglass of the ETS-VIII solar array is a microsheet with a blue-red reflector coating for silicon cells whose thickness is 100 μm. The capacitance of the coverglass and adhesive for one string (262 cells) of the solar array is 180 nF. ETS-VIII consists of two wings for the solar array. Each wing has 44 array strings and an 8-μF coverglass capacitance.

Figure 4 shows a photograph of a solar-array coupon. The solar-array coupon contains three strings that are referenced as R, B, and G, respectively. Each string consists of five Si cells (3.5×7 cm) with a thickness of 100 μm. We assign a number to each cell from left to right in one string, as shown in Fig. 4. The cells are mounted on a Kapton substrate with a thickness of 50 μm having a capacitance of 60 pF per cell. The Kapton film is mounted on a carbon-fiber-reinforced plastic face sheet substrate (0.1 mm thick) on the top of an aluminum honeycomb plate (2.5 cm thick). All of the side edges of the coupon panel are covered with Kapton film to prevent arcing. The solar-array string terminals are connected to the cables through the bus bars, which are coated with RTV. The cable of each string is shortened and connected to the high-voltage feed-through at the chamber wall.

Two coupons, thick-2 and thin-1, were baked at 125°C for 5 h in the chamber, which was different from the chamber where the experiments were conducted, at the factory. The coupon thick-1 was not baked. No special treatment to the array surface was provided after the array coupons were shipped from the factory to the laboratory. Each time the array coupon was exposed to atmosphere, the coupon was baked at a constant temperature of $70°C \pm 1°C$ at least for two hours in vacuum (10^{-4} torr). The array temperature during the experiment was maintained at $40°C \pm 1°C$.

External Circuit

A diagram of the experimental circuit is shown in Fig. 5. Table 1 lists the parameters for each case. The circuit was outside the vacuum chamber and was connected to the solar array via a high-voltage

Table 1 Experimental conditions

Case no.	Experimental duration, h	Beam energy, kV	Neutral density $\times 10^{16}$ m^{-3}	Coupon
1	20	3.5 ~ 5	4	Thick-1
2	20	4.6 ~ 5	9	Thick-2
3	10	5	9	Thick-2
4	20	4.9, 5	9	Thin-1

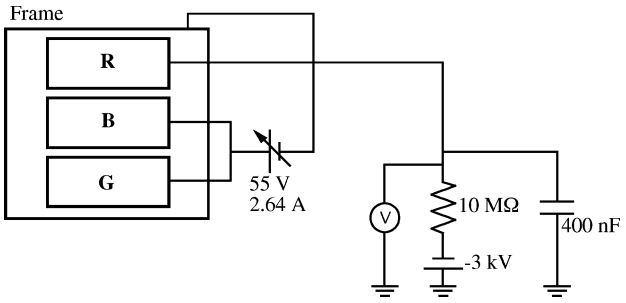

a) Cases 1 and 2

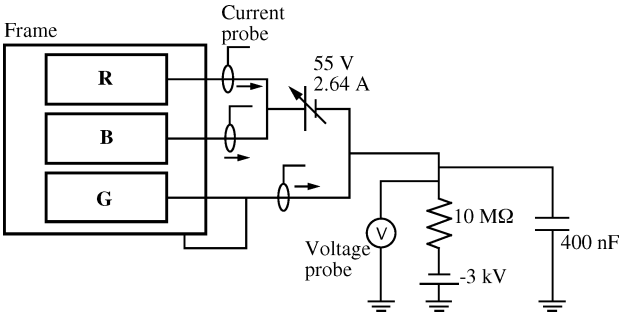

b) Case 3

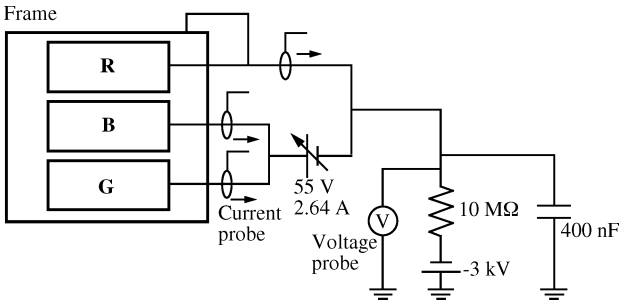

c) Case 4

Fig. 5 Diagram of electrical circuit.

feedthrough. We biased the solar array to a high negative potential of −3 kV using a high-voltage power supply, connected through a 10-M resistor. The potential of the solar array was measured using a high-voltage (HV) probe. Each string of the coupon was separately biased. The different bias values were used to represent the maximum potential difference between different cells of the same string on the flight array. The frame and one string were biased to −3 kV, and two of the strings were biased +55 V with respect to the frame. To apply the interstring and string-substrate voltage of 55 V, we used a floating power supply. The maximum current to flow was limited to 2.64 A. The power supply worked as a constant voltage supply. But during a short circuit like that from sustained arc, it works as a constant current supply with the maximum current limited to a present value of 2.64 A. We measured the currents to R, B, and G strings of the array using current probes (100 MHz). The current probes and the HV probe were connected to a four-channel oscilloscope (100 MHz), which was triggered by the rise of HV probe signal.

Electrons produced by an arc on the solar array propagate and neutralize the positive charge stored on the coverglass. The charge neutralized by the electrons returns to the arc position through the solar-array circuit, and the electrostatic energy is given to the arc plasma via the joule heating. To simulate this energy source, we inserted an additional capacitance in the external circuit. In the previous experiments, a trigger arc occurred under the inverted gradient condition when the potential difference between the surface of coverglass and the interconnector was higher than 400 V (Ref. 3). The capacitance of the ETS-VIII solar arrays is 16 μF (two wings). The energy stored in solar arrays becomes 1.8 J at the potential difference of 400 V. In the present experiment, we use an external capacitance of 400 nF at −3 kV bias voltage to simulate the worst case in orbit.

Results and Discussion

Twenty-Hour Test of Thick Coupon

In case 1, 20 experiments were carried out, each for 1 h with a total experimental duration of 20 h carried out over four days. Each experiment had a minimum interval of 2 min and maximum of 15 h. During the 20 h the vacuum chamber was kept closed, we observed 423 trigger arcs during the 20-h experiment. The potential difference between the coverglass and the cell increases with decreasing potential difference between the electron and the coverglass. If the potential difference between the coverglass and the cell increases, the arc rate also increases. In the experiment, the energy of electron beam was reduced gradually from 5 to 4 kV to maintain the arc rate because the arc rate decreased as the experiment went on at constant beam energy.

The locations of arcs are shown in Fig. 6. These were identified by the arc location identification system. The distribution of arcs

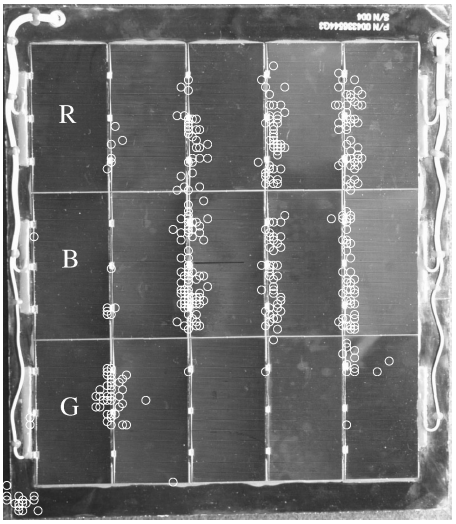

Fig. 6 Distribution of arc locations in case 1. Each arc location was identified from the video image.

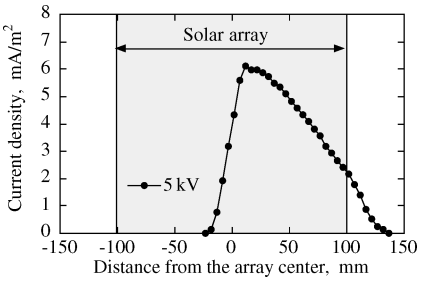

Fig. 7 Distribution of current density for the electron beam on B string of a solar-array coupon.

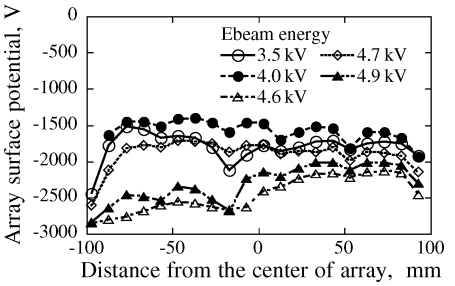

Fig. 8 Distribution of array surface potential along the centerline of array after experiments in case 1.

was within a circle on the solar-array coupon. Figure 7 shows the distribution of current density of electron beam. This distribution was measured on the B string along the center axis of the vacuum chamber using the probe with a diameter of 10 mm. As shown in Fig. 7, the distribution of current density of the electron beam corresponded to the distribution of arc location along the B string. The reason we have some arcs between no. 1 and 2 cells of the G string is probably the side lobe of the electron beam pattern. In another test, we had confirmed the electron beam has small side lobes. Figure 8 shows the distributions of solar-array surface potential after the experiments. The potential distribution was measured on the B string along the center axis of the chamber with a distance of 5 mm between the potential probe and the array surface taken within 5 min after each experiment. The potential probe showed the average potential at the surface of the solar array within 25 mm in diameter. The probe was moved at intervals of 10 mm along the center axis of the vacuum chamber. The surface of the solar-array coupon was charged uniformly. The maximum potential difference between the coverglass and interconnectors was 1.5 kV.

In spite of the many arcs occurring at the interstring gap between R and B strings, which had a bias voltage of 55 V, the interstring sustained arc did not occur. The string-substrate sustained arc also was not observed between B and G strings and the substrate. Therefore, the thick coupon had enough insulation strength to prevent sustained arcs even if many trigger arcs occurred during the experiment. On the other hand, we observed that the coverglass surface was contaminated.

Figure 9 shows a photograph of the solar-array surface covered with contamination. Analysis by electron-probe microanalysis showed that the contamination was mainly composed of silicone of which RTV was made. The pattern of the contamination was very similar to that of arc position and distribution of electron beam density (Fig. 7).

Table 2 lists the electrical performance of the coupon after the experiment. The electrical performance of the solar array was measured using a xenon flash lamp. In the table, I_{sc} represents the short-circuit current and P_{max} represents the maximum output power under various loads. The electrical performance was measured both after the experiment and after removal of the contamination from the surface of strings B and G. The contamination of the R string was not cleaned. The strings R and B showed decrease in both I_{sc} and P_{max}

Table 2 Change in electrical output resulting from experiments and cleaning for case 1[a]

	I_{sc}			P_{max}		
String	Before exp., A	After exp., %	After cleaning, %	Before exp., W	After exp., %	After cleaning, %
R	1.097	−1.9	NA	2.53	−5.5	NA
B	1.094	−2.8	−0.6	2.52	−6.3	−2.7
G	1.095	−0.6	−0.6	2.49	−18.1	−18.1

[a]The differences from the value before experiments are listed. The typical errors in measurement are 0.0013 A and 0.013 W.

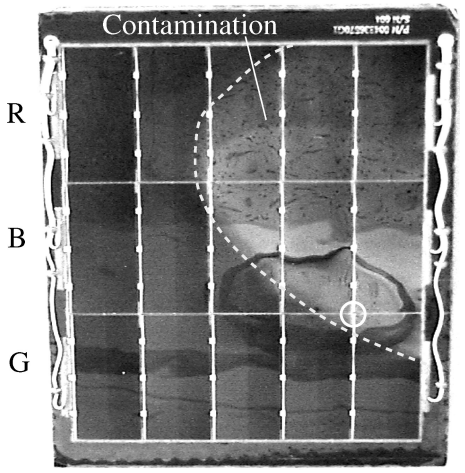

Fig. 9 Photograph of the contaminated array surface after experiment in case 1.

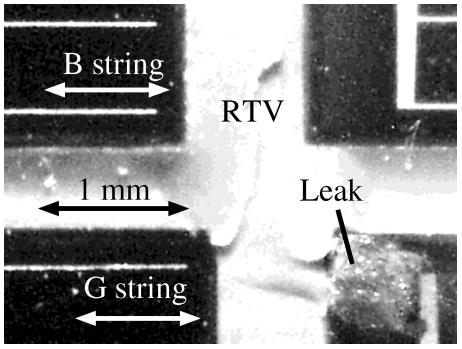

Fig. 10 Microscope picture of a broken cell in case 1. The position on the array coupon is denoted by a white circle in Fig. 9.

after the experiment. But after the cleaning, the I_{sc} of string B recovered. This suggests that the contamination on coverglass decreased the light flux incident to the cells.

The decrease in I_{sc} was larger for strings R and B than for string G. This result agreed with the contamination pattern where most of the contamination covered the string R and B as shown in Fig. 9. The string G showed little decrease in I_{sc}. However, P_{max} of string G had decreased by 18% and did not recover even after cleaning. Therefore the power drop of string G did not depend on the contamination. The fact that the drop of P_{max} was 18% suggested that one cell of the five cells in string G was broken and short circuited. Because the string still generated the power, it was not open circuited.

Optical-beam-induced resistance change (IR-OBIRCH) analysis was applied to string G. In IR-OBICH, the current leaking point is identified from the change of resistance of samples when a spot of laser beam is applied to the surface and the temperature of the coupon rises locally. From the result of IR-OBICH, it was confirmed that the current leaked at the cell that was next to the bus bar. The microscope picture of this current leaking point is shown in Fig. 10. This position is marked by a white circle in Fig. 9. The current

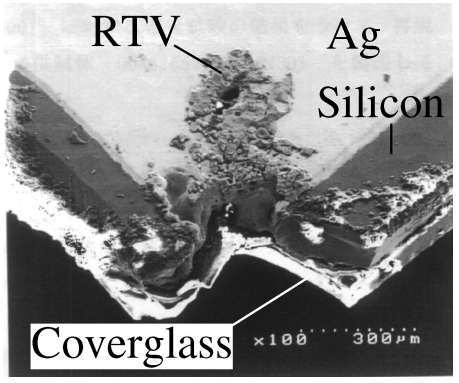

Fig. 11 Scanning electron microscope picture of the damaged cell removed from Kapton substrate. This picture was taken from the backside of the cell.

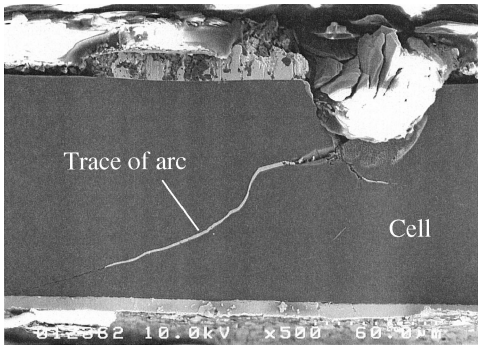

Fig. 12 Scanning electron microscope picture of the cross section at the current leak point.

leaking point looked damaged, and the surface color changed from black to gray. However, the RTV was not damaged, though the damage at the current leaking point was significant. An arc track was observed on the cell from a visual observation. Pictures of the broken cell were taken by scanning electron microscope (SEM). The cell corner shown in Fig. 10 (denoted as Leak) was very fragile and peeled off during handling.

An arc track was observed to run between the coverglass and the cell from the edge to the silver N electrode. This type of arc track has not been reported before in the literature. Figure 11 was taken from the back of the cell. The protuberance produced by the arc was on the center of the picture. From the SEM pictures, we conclude that the current leak is the result of the destruction of the positive–negative (PN) junction. Because the current leak position is away from P+ dot layer of IBF, the leak is not related to IBF.

The broken cell was cut, and a cross-sectional picture of the arc track was taken. Figure 12 shows an SEM picture of the arc track, where the top is the coverglass side (but not shown in the figure) and the bottom is the substrate side. The figure shows that the arc track runs from top to the bottom. The cross section is away from the protuberance of the back electrode shown in Fig. 11. Energy-dispersive x-ray spectroscopy identified a trace of silver along the arc track, which clearly indicates that it was produced by arcs.

Thick and Thin Coupons

To investigate whether the contamination and the cell destruction were reproducible for other coupons, we conducted an experiment with a duration of 30 h under the same conditions as case 1 using a virgin thick coupon, thick-2. We also conducted a 20-h experiment using a thin coupon to examine whether the contamination and the cell damage were the phenomena peculiar to a thick coupon. The 30-h experiment with thick-2 coupon was divided into 20 h (case 2) and 10 h (case 3). After the initial 20 h (case 2), the coupon was taken out from the chamber for measurement of its electrical output.

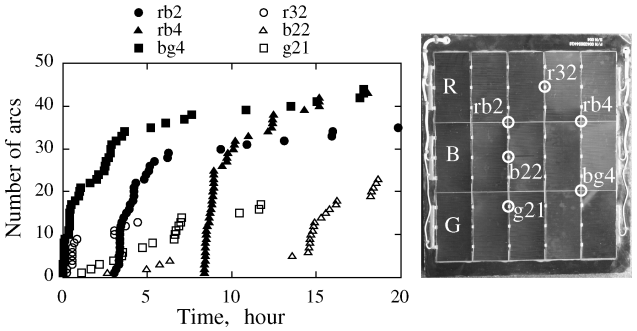

Fig. 13 Time history of arcs in case 2.

Then it was tested for another 10 h. The number of arcs was 332 in case 2 and 149 in case 3. The 20-h experiment with a thin coupon (case 4) had 391 arcs. The experiment for case 2 was divided into 10 measurements of 2 h respectively. Cases 3 and 4 were divided into 6 and 4 h. The arc rate of every case decreased with time as in case 1.

The locations of 65 arcs, out of a total of 391 arcs in case 4, could not be identified because of malfunction of image recording system. From the arc-location measurements, the distribution of arc location coincided with that of the electron beam as in case 1. The position of the array coupon inside the chamber was kept the same for all of the four cases. From these results, arcs were likely to occur at places where the electron beam irradiated. Many arcs occurred between strings in cases 2 and 3. It was thought that the thick coupon could suppress arcs between strings. However, fewer arcs occurred between strings in case 4 that used the thin coupon. The arcs occurred at thickly grouted string gaps probably because thicker RTV grouting had more risk of void formation inside the RTV layer, thus producing more points of weak electrical insulation. Visual observation by optical microscope revealed many voids in the RTV grouting between strings. No matter how carefully done, there is always a chance of inclusion of air in the RTV layer, which becomes the source of a void after the RTV is exposed in vacuum. Voids are usually the starting point of failures in electrical insulation in solids.

The arc rate at each position in case 2 is shown in Fig. 13. The locations rb2, rb4, and bg4 correspond to the points between strings where many arcs occurred. The positions r32, b22, and g21 correspond to the interconnectors where many arcs occurred. As shown in this figure, the arc rate was high between strings, with up to about between 30 and 40 arcs, but slowed down later. Arcs at interconnectors also occurred successively, but they slowed down sooner than arcs between strings. The thick-1 coupon had the same tendency.

Arcs easily followed after an arc occurred at the gap between strings. When arcs occur, the RTV evaporates because of the heat. Therefore the RTV gas could easily be generated at the interstring region where a RTV was grouted thickly. This raises the gas density and the number of arcs near the triple junction.

Arcs between strings tended to have the largest flash size. In the case of arcs occurring at interconnectors, the size of flash tended to be small. Many large arcs occurred in both the R-B interstring and B-G interstring region. Therefore, the large arcs did not result from the interstring bias voltage. The arcs between strings had a large flash because the RTV silicon was easily evaporated and excited by the arcs between strings.

For cases 3 and 4, the contamination was observed on the array surface regardless of the coupon types, insulation reinforced or standard. The pattern of the contamination was identical among the three coupons. These results suggested the contamination pattern depends on the arc position and electron-beam pattern. From visual observation, the contamination of the thin coupon was thinnest.

Figure 14 shows typical waveforms of arc current observed in the experiment. There was no significant difference in appearance between the thick coupon and thin coupon. Table 3 lists the peak current and the amount of charge transferred by the arc current in cases 3 and 4. There was no significant difference in the peak current

Table 3 Peak current and transferred charge in cases 3 and 4[a]

	Peak current, A		Charge, mC	
Parameter	Case 3	Case 4	Case 3	Case 4
Mean	42	44	0.42	0.40
Maximum	97	108	0.58	0.76
Minimum	17	17	0.14	0.08
Standard deviation	17	16	0.08	0.09
Data points	139	375	139	375

[a]The typical errors in measurement are 1 A and 0.01 mC.

Table 4 Background pressure rise as a result of arcing[a]

	Pressure increment, $\times 10^{-4}$ Pa		
Parameter	Case 2	Case 3	Case 4
Mean	3.69	3.73	3.27
Maximum	6.07	5.08	4.52
Minimum	2.43	2.40	1.33
Standard deviation	0.40	0.47	0.40
Data points	266	98	392

[a]The typical error in measurement is 0.003×10^{-4} Pa.

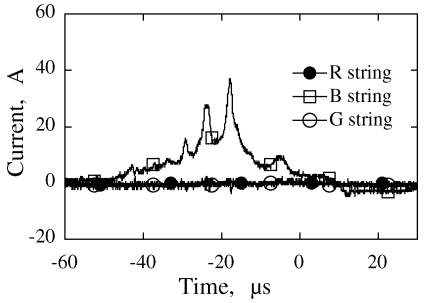

Fig. 14 Typical waveform of the arc current in case 3.

and the charge between cases 3 and 4. Therefore, the arc current was independent of the amount of RTV applied to the coupons. The amount of electrical charge transferred was approximately 0.4 mC, although the external capacitance could supply an electric charge of up to 1.2 mC to the arc.

The chamber background pressure was monitored during experiments and observed that the background pressure increased when an arc occurred. Figure 15 shows an example of the temporal variation in the background pressure. The background pressure was measured at a sampling rate of approximately five samples per a second using an ionization vacuum gauge installed between the chamber and a turbomolecular pump. Figure 15a shows the temporal variation of the pressure in case 2 for the duration of 2 h. The pressure increased sharply when an arc occurred. Figure 15b shows an enlarged chart of Fig. 15a. Table 4 lists the pressure jump due to arcing. The pressure jump for the thick coupon (cases 2 and 3) was higher than that of thin coupon (case 4). Because the thick coupon has a thick layer of RTV even under interconnectors as well as between strings and below cells, a large amount of RTV silicon is vaporized as a result of an arc wherever the arc occurs. Therefore, the difference in the amount of contamination between different types of coupon is caused by the difference in the amount of RTV silicon applied in the coupon.

Table 5 lists the electrical output after experiments and cleaning. After experiments, the R string was cleaned in case 3, and all strings were cleaned in case 4. Maximum output power decreased in every case after tests using the electron beam. In cases 2 and 3, although the R and B string had a significant power drop, the G string had little drop. This power drop is because the contamination covered mostly over the R and B strings.

The power reduction of the thin coupon (case 4) was much smaller than that of the thick coupon (cases 2 and 3), although

Table 5 Change in electrical output after experiments in cases 2–4[a]

Case	String	Status	P_{max}, %	I_{sc}, %
2	R	After test	−4.8	−0.4
	B		−7.7	−2.2
	G		−0.8	−0.1
3	R	After test	−6.5	−1.0
		After cleaning	−2.8	0.1
	B	After test	−15.9	−2.2
	G	After test	−0.8	0.0
4	R	After test	−0.8	0.0
		After cleaning	2.1	−0.6
	B	After test	−5.4	−2.2
		After cleaning	−3.8	0.0
	G	After test	−0.4	−0.1
		After cleaning	0.0	0.2

[a]The differences from the value before experiments are listed.

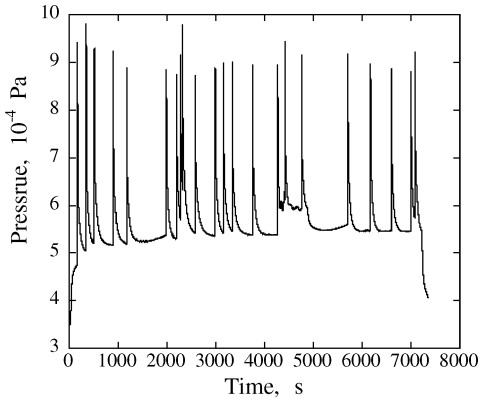

a)

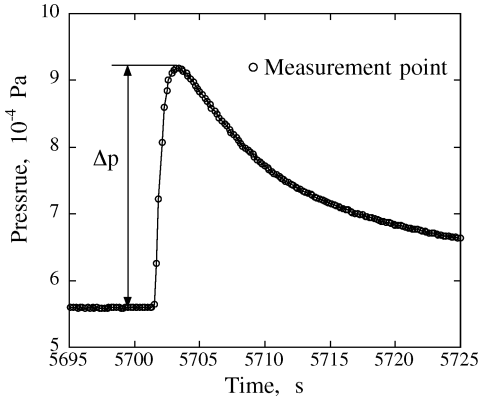

b)

Fig. 15 Typical background pressure rise as a result of arcing.

the contamination accumulated on the coverglasses in case 4 in the same way as cases 1, 2, and 3. From this result, it is confirmed that the contamination on the thin coupon was much thinner than that on the thick coupon. The B string had a larger power drop than other strings in case 4. After cleaning, I_{sc} of all strings recovered; however, only the P_{max} of string B still remained low. The recovery of I_{sc} denotes that the contamination has been removed completely, and this result shows that at least one cell was damaged as a result of arcs.

Figure 16 shows the electrical output of the solar array after the experiment in cases 2 and 3. The decrease of the electrical output is plotted against the number of arcs in this figure. The electrical output decreased as the number of arcs increased. Both I_{sc} and P_{max} of string R decreased with the number of arcs in case 3. In string B, P_{max} decreased with the number of arcs although I_{sc} was constant. This suggests that one cell in string B was also damaged by arcing as in case 1. By measuring the electrical output for each cell in string

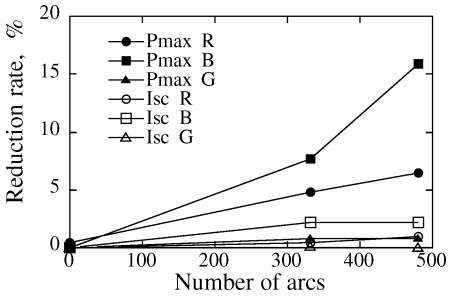

Fig. 16 Relation between the reduction rate of electrical output and number of arcs.

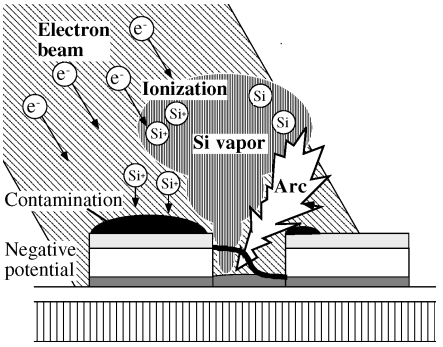

Fig. 17 Schematic picture of model of contamination adhesion.

B, the damaged cell was identified to be the no. 5 cell at the right side. A large arc spot was found between the strings B and G along the damaged cell.

Discussion

Mechanism of Contamination

A model of contamination is shown in Fig. 17. An arc occurs at the side edge of a cell at either the interconnector or interstring gap, and a large arc current flows. The temperature increases locally at the arc position as a result of the arc current, and the RTV silicon is vaporized near the arc position. The silicon vapor diffuses outside and is ionized via collision with the electron beam forming positive ions. Silicone ions are attracted back to the coverglass, which has a negative potential, and attach to the coverglass surface. Therefore, the contamination pattern matches the pattern of electron beam on the solar-array surface. It is difficult for the contamination to attach to the area outside the electron-beam envelope because even if the silicone vapor is produced via the arc it is not ionized. The reason we see little contamination near arc positions between no. 1 and 2 cells of string G caused by the side lobe of electron beam is unknown. Probably the narrow-beam cross section or small-beam current density at that point had some effect.

According to this model, as long as the vapor can be ionized near the array surface, ions can be attracted back to the array with a negative potential and contaminate the coverglass surface. Therefore, there is a possibility that the vapor is ionized not only by high-energy electrons but also by UV light in orbit.[6]

The coupon suffered a 6% reduction in the electrical power as a result of contamination in cases 1 and 3. In case 4, the power drop was insignificant. The excessive RTV application on the thick coupon resulted in the power reduction because of the contamination. Therefore, applying too much RTV silicon should be avoided.

Damage of Cell

Cells were damaged in all coupons. The damaged positions of cells were identified for thick-1 and thick-2. The cell next to the P bus bar, that is, no. 5, was damaged in both coupons though the string of the damaged cell was different in thick-1 and thick-2. The coverglass side of a cell is the N electrode, and the substrate side

is the P electrode. The arc traveled between the coverglass and cell and penetrated the cell causing damage to the PN junction.

The damaged position for thick-1 is near the interstring gap between B and G strings, where no interstring bias voltage was applied (see Fig. 5). From this result, the cell's damage was not the result of the interstring bias voltage. This fact suggests that similar cell damage can occur on any solar array in GEO regardless of its operational voltage. Unlike the sustained arc, however, this damage alone does not cause serious degradation of the power system because only one cell is short circuited leading to the decrease of output voltage by a factor equal to the ratio of one cell to the total number of cells (typically 100 or more) in one string. Therefore, this phenomenon might have been unnoticed previously because the observable power reduction caused by one cell damage was probably too small to lower the string output voltage below the regulated voltage.

Although it was not observed in the ground tests, there is still a possibility that trigger arcs might lead to a string-substrate sustained arc. The arc trace is observed to run through the cell and penetrate through the N electrode in the backside (see Figs. 11 and 12). We cannot rule out the possibility that the arc trace further penetrates the Kapton layer and causes a short circuit between the cell electrode and the substrate if that point of Kapton sheet has already been damaged by other mechanisms.

Conclusions

Ground tests of the solar-array coupons intended for the ETS-VIII satellite were carried out under the inverted gradient condition using an electron beam. A thick coupon was proposed to reinforce the electrical insulation based on previous tests of the ETS-VIII array.[3,4] The coupon has a thicker RTV layer below the cells and all of four edges of cell are covered extensively by room-temperature vulcanization (RTV). As a comparison a thin coupon with minimum RTV grouting was also tested. In the two tests with a duration of 20 h on the thin coupon and 30 h on the thick coupon, neither an interstring nor string-substrate sustained arc occurred for the thick coupon, and we verified the insulation capability of the thick coupon. Making RTV silicone coating thicker, however, is not a perfect solution to the arcing problem. We have seen many trigger arcs occurring between string gaps, which have been extensively grouted by thick layer of RTV. We also observed an electric power reduction for the thick coupon. This electrical power drop for the coupon resulted from contamination on the coverglass and the cell damage. The cell damage is the result of a short circuit of the PN junction.

From the 30-h experiment on the thick coupon and of 20 h on the thin coupon, it was confirmed that both the contamination and the cell damage can occur for any type of coupon, though the electric power drop for the thick coupon was larger than that of the thin coupon. This is because that the amount of contamination increased with the increasing amount of RTV silicone adhesive on the coupon. Silicon vapor produced by arcing was ionized by the electron beam and attached to the coverglass as contamination. In orbit, contamination can occur not only by high-energy electrons but also by UV radiation. Therefore, one should avoid excessive RTV application on coupon.

The advantage of using a thick RTV layer between the cell and the Kapton is that it can give an extra safety margin against short circuits between the cell and the carbon-fiber-reinforced plastic (CFRP) substrate even if the arc damages the back side of the cell. We have seen an arc trace that runs between the top and the bottom of a cell. There is a possibility that the arc trace runs further through a defect in the Kapton to the underlying CFRP substrate leading to a string-substrate sustained arc.

Based on the test results, the final design of solar array for the ETS-VIII satellite was defined. To avoid the contamination, the amount of RTV at interstring gaps and below interconnector should be minimal so that the RTV layer works against the sustained arc but produce little contamination. Therefore the amount of grouting of the interstring gap is specified to be the same as that for the thin coupon. The RTV layer between the cell and the Kapton substrate is specified to be the same as that for the thick coupon to have enough insulation between strings and substrate to prevent the worst case of a string-substrate sustained arc.

Acknowledgments

The authors thank the members of NEC Toshiba Space Systems for the array sample fabrication and after-experiment analysis. The authors also thank M. Hikita of Kyushu Institute of Technology and S. Kawakita of the National Space Development Agency of Japan for their useful comments.

References

[1]Katz, I., Davis, V. A., and Snyder, D. B., "Mechanism for Spacecraft Charging Initiated Destruction of Solar Arrays in GEO," AIAA Paper 98-1002, Jan. 1998.

[2]Meguro, A., Tsujihata, A., Hamamoto, N., and Homma, M., "Technology Status of the 13 m Aperture Deployment Antenna Reflectors for Engineering Test Satellite VIII," *Acta Astronautica*, Vol. 47, No. 2, 2000, pp. 147–152.

[3]Cho, M., Matsumoto, T., Ramasamy, R., Toyoda, K., Nozaki, Y., and Takahashi, M., "Laboratory Tests on 110V Solar Arrays in a Simulated Geosynchronous Orbit Environment," *Journal of Spacecraft and Rockets*, Vol. 40, No. 2, 2003, pp. 211–220.

[4]Ramasamy, R., Cho, M., Nozaki, Y., and Takahashi, M., "Laboratory Tests on 110-Volt Solar Arrays in Ion Thruster Plasma Environment," *Journal of Spacecraft and Rockets*, Vol. 40, No. 2, 2003, pp. 221–229.

[5]Bogus, K., Claassens, C., and Lechte, H., "Investigations and Conclusions of the ECS-Solar-Array in-Orbit Power Anomalies," *Proceedings of the 18th Inst. of Electrical and Electronics Engineers Photovoltaic Space Conference*, IEEE Publications, Piscataway, NJ, 1985, pp. 368–375.

[6]Tribble, A. C., Boyadjian, B., Davis, J., Haffner, J., and McCullough, E., "Contamination Control Engineering Design Guidelines for the Aerospace Community," NASA CR4740, May 1996.

N. Gatsonis
Associate Editor